Organic Electronics 14 (2013) 1621–1628

Contents lists available at SciVerse ScienceDirect

Organic Electronics

journal homepage: www.elsevier.com/locate/orgel

A strategy to enhance both V_{OC} and J_{SC} of A–D–A type small molecules based on diketopyrrolopyrrole for high efficient organic solar cells

Yoon Suk Choi, Won Ho Jo *

Department of Materials Science and Engineering, Seoul National University, 1 Gwanak-ro, Gwanak-gu, Seoul 151-744, Republic of Korea

ARTICLE INFO

Article history:
Received 18 February 2013
Received in revised form 13 March 2013
Accepted 23 March 2013
Available online 6 April 2013

Keywords:
Photovoltaics
Small molecule
Diketopyrrolopyrrole
HOMO
Fused aromatic ring

ABSTRACT

Four different diketopyrrolopyrrole (DPP)-based small molecules (SMs) with A–D–A type structure were synthesized, where electron-donating unit (D) was systematically varied with different electron-donating power (thiophene vs. phenylene; thienothiophene vs. naphthalene) and different molecular planarity (bithiophene vs. thienothiophene; and biphenylene vs. naphthalene). The small molecules with weak donating unit (phenylene or naphthalene) have deeper HOMO energy levels than those with strong donating unit (thiophene or thienothiophene), and thus exhibit higher V_{OC}. When the fused aromatic ring (thienothiophene or naphthalene) with planar molecular structure is introduced in SMs, the SMs exhibit high hole mobility and thus afford high J_{SC}. As a result, the introduction of naphthalene (weak donating power and planar structure) enhances both V_{OC} and J_{SC}, resulting in a promising power conversion efficiency of 4.4%. This result provides a valuable guideline for rational design of conjugated small molecules for high performance organic solar cells.

1. Introduction

Solution processable polymer solar cells based on bulk heterojunction (BHJ) concept have intensively been investigated as printable and roll-to-roll processable energy devices for their advantages of low cost, flexibility and large area fabrication [1–8]. Especially, considerable efforts have been made to design new conjugated polymer materials with broad light absorption and suitable frontier orbital energy levels [9,10]. However, conjugated polymers are subjected to inevitable drawbacks such as batch-to-batch variation of molecular weight, broad polydispersity and complicated purification.

As a promising alternative to polymer solar cells, small molecular organic solar cells have recently been developed because of their characteristic advantages of well-defined molecular weight, synthetic reproducibility, and simple purification process. A number of small molecules (SMs) have been developed as donor components for BHJ organic solar cells, and the power conversion efficiency (PCE) has achieved over 6.0% [11–14]. However, the PCEs are still lower than those of polymer solar cells (over 8%) [15–18]. Thus, further works on designing molecular structure are needed for improving the solar cell performance.

Owing to intensive studies on the ideal donor material in BHJ organic solar cells for the past decade, some requirements for high performance organic solar cells have been established: (1) broad and strong light absorption in the visible region, (2) high hole mobility for fast charge carrier transport to yield high short-circuit current (J_{SC}), and (3) suitable energy levels to ensure high open-circuit voltage (V_{OC}) and efficient exciton dissociation [19]. Broad absorption is requisite for efficient solar cells. One of effective strategies to broaden light absorption is to synthesize organic molecules with low optical bandgap through combination of electron-donating (D) and electron-accepting (A) units in alternative sequence, where the highest

* Corresponding author. Tel.: +82 2 880 7192; fax: +82 2 876 6086.
E-mail address: whjpoly@snu.ac.kr (W.H. Jo).

1566-1199/$ - see front matter © 2013 Elsevier B.V. All rights reserved.
http://dx.doi.org/10.1016/j.orgel.2013.03.031

occupied molecular orbital (HOMO) and the lowest unoccupied molecular orbital (LUMO) energy levels of D–A type molecules become higher and lower than those of D and A molecules, respectively. Considering that the LUMO energy level of a typical acceptor, [6,6]-phenyl-C_{61}-butyric acid methyl ester ($PC_{61}BM$) is about −4.0 eV, the LUMO energy level of donor molecule should be higher than −3.7 eV, which limits lowering the bandgap [20], because the LUMO level offset between donor and acceptor should be larger than 0.3 eV for efficient exciton dissociation. On the other hand, raising the HOMO energy level for lowering the gap leads to decrease in V_{OC}, because the V_{OC} is proportional to the difference between the HOMO energy level of donor and the LUMO energy level of acceptor. Hence, the lowering of bandgap may sacrifice the V_{OC}. As a consequence, a new strategy to overcome this trade-off behavior should be developed for high performance solar cells.

Another method to improve J_{SC} is to incorporate planar molecular structure [21,22], because the molecules with planar structure are efficiently packed for crystallization which enhances the charge carrier mobility. For this purpose, fused aromatic units have been incorporated in π-extended molecular backbone [23–26]. Recently, conjugated alternating copolymers based on fused aromatic ring such as thieno[3,2-b]thiophene (TT) [27] and naphthalene (NPT) [28] have exhibited high charge carrier mobility in FET device up to 0.79 $cm^2 V^{-1} s^{-1}$ and 0.98 $cm^2 V^{-1} s^{-1}$, respectively.

Diketopyrrolo[3,4-*c*]pyrrole (DPP) has emerged as an effective electron-deficient building block of low bandgap conjugated organic molecules for organic solar cells. The planarity of DPP, strong absorption in near-infrared region and its high optical density render the DPP unit suitable for high performance photovoltaics [29–31]. Recently, DPP-based SMs with D–A–D or A–D–A structure have exhibited promising PCEs [32–35]. Particularly, Marks and co-workers [33] synthesized a small organic molecule with A–D–A structure, where A and D are DPP and naphthodithiophene, respectively, and reported a PCE of 4% when blended with $PC_{61}BM$. Recently, we reported A–D–A type SMs where A is DPP and D is simple donating units such as thiophene and phenylene [36]. When phenylene was used as D unit, the HOMO energy level of the SM was deeper and thus the V_{OC} of photovoltaic cell was increased, yielding a PCE of 4%.

In this work, to overcome the trade-off between J_{SC} and V_{OC}, we designed four different SMs with A–D–A type structure, where A is thiophene-capped DPP (TDPP) and D is electron-donating unit such as bithiophene (T2), biphenylene (Ph2), thienothiophene (TT) and naphthalene (NPT), as shown in Fig. 1, where TT and NPT are the corresponding fused aromatic rings of T2 and Ph2, respectively. Here, it is expected that the use of weak donor increases V_{OC} while the introduction of fused aromatic ring increases J_{SC} as well. Since the electron-donating capability of Ph2 and NPT are weaker than T2 and TT, respectively, $Ph2(TDPP)_2$ and $NPT(TDPP)_2$ exhibit deeper HOMO energy levels than $T2(TDPP)_2$ and $TT(TDPP)_2$ and thus larger V_{OC}, while the introduction of fused aromatic rings (TT and NPT) instead of T2 and Ph2 increases J_{SC} due to planarity of SMs. Consequently, $NPT(TDPP)_2$ with

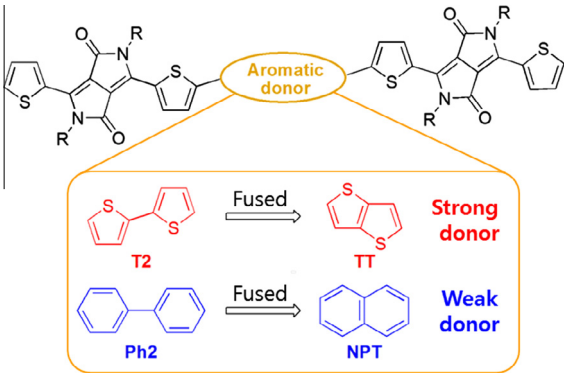

Fig. 1. Chemical structures of DPP-based small molecules.

weak electron-donating and fused aromatic ring exhibits a PCE of 4.4% with the highest V_{OC} of 0.87 V and the highest J_{SC} of 9.5 mA cm^{-2} when blended with $PC_{71}BM$ as active layer in BHJ solar cells.

2. Experimental section

2.1. Materials

3-(5-Bromothiophene-2-yl)-2,5-bis-(2-ethylhexyl)-(6-thiophene-2-yl)pyrrolo [3,4-*c*]pyrrole-1,4(2*H*,5*H*)-dion (1) [37], 5,5′-bis(trimethylstannyl)-2,2′-dithiophene (2) [38], 2,5-bis(trimethyl-stannyl)thieno[3,2-*b*]thiophene (3) [27], 4,4′-Bis(4,4,5,5-tetramethyl-1,3,2-dioxaborolan-2-yl)-biphenyl (4) [39], and 2,6-bis(4,4,5,5-tetramethyl-1,3,2-dioxabrolan-2-yl)-naphthalene (5) [28] were synthesized following the same procedure as reported in the literature. $Pd(PPh_3)_4$, *N*-bromosuccinimide (NBS), Aliquat 336 and 2-ethylhexyl bromide were purchased from Sigma–Aldrich and used without further purification. Common organic solvents were purchased from Daejung. Tetrahydrofuran was dried over sodium/benzophenone under nitrogen (N_2) and freshly distilled prior to use. Poly(3,4-ethylenedioxythiophene):poly-(styrene sulfonate) (PEDOT:PSS) (Clevios P VP AI 4083) was purchased from H.C. Stark and passed through a 0.45 μm PVDF syringe filter before spin-coating. $PC_{71}BM$ was obtained from Nano-C. All other reagents were purchased from Tokyo Chemical Industry and used as received.

2.2. Synthesis

2.2.1. Synthesis of $T2(TDPP)_2$

$T2(TDPP)_2$ was synthesized by the Stille coupling. After the compound 1 (200 mg, 0.33 mmol), 2 (81 mg, 0.17 mmol) and $Pd(PPh_3)_4$ (19 mg, 0.02 mmol) were dissolved in toluene (10 mL) under N_2 atmosphere, the reaction mixture was stirred at 110 °C for 24 h and then cooled down to room temperature. The reaction mixture was poured into acidic methanol (200 mL methanol and 10 mL HCl) and stirred for 1 h to remove the metal catalyst. The crude product was obtained by vacuum filtration and purified by column chromatography on silica gel (100% $CHCl_3$ as eluent) to yield $T2(TDPP)_2$ as a deep blue solid

(160 mg, 80% yield). ^{1}H NMR (300 MHz, $CDCl_3$,δ): 8.94 (d, *J* = 4.1 Hz, 2H), 8.91 (d, *J* = 3.9 Hz, 2H), 7.66 (d, *J* = 4.8 Hz, 2H), 7.45 (d, *J* = 4.3 Hz, 2H), 7.30 (d, *J* = 4.1 Hz, 2H), 7.28–7.26 (m, 6H), 4.06–3.98 (m, 8H), 1.92–1.88 (m, 4H), 1.38–1.20 (m, 32H), 0.92–0.87 (m, 24H); ^{13}C NMR (500 MHz, $CDCl_3$,δ): 161.7, 161.6, 142.0, 134.0, 139.7, 137.3, 136.8, 135.5, 135.3, 130.5, 129.9, 128.4, 128.4, 126.0, 125.1, 124.8, 108.3, 108.2, 46.0, 39.3, 30.4, 30.3, 28.6, 28.4, 23.7, 23.6, 23.1, 23.1, 14.1, 14.0, 10.6, 10.5; MALDI-TOF MS *m*/*z*: calcd for $C_{68}H_{82}N_4O_4S_6$, 1211.8; found, 1211.8.

2.2.2. Synthesis of TT(TDPP)$_2$

The same procedure as for T2(TDPP)$_2$ was performed. When the compound 1 (200 mg, 0.33 mmol) was reacted with 3 (80 mg, 0.17 mmol) in the presence of $Pd(PPh_3)_4$ (19 mg, 0.02 mmol), the product TT(TDPP)$_2$ was obtained as a deep blue solid (170 mg, 86% yield). ^{1}H NMR (300 MHz, $CDCl_3$,δ): 8.93 (d, *J* = 4.2 Hz, 2H), 8.90 (d, *J* = 3.8 Hz, 2H), 7.62 (d, *J* = 4.9 Hz, 2H), 7.45 (s, 2H), 7.35 (d, *J* = 4.2 Hz, 2H), 7.28 (s, 2H), 4.04–4.00 (m, 8H), 1.91–1.87 (m, 4H), 1.39–1.25 (m, 32H), 0.94–0.83 (m, 24H); ^{13}C NMR (500 MHz, $CDCl_3$,δ): 161.7, 142.4, 140.2, 140.1, 139.5, 138.8, 136.6, 135.3, 130.6, 129.9, 128.7, 128.5, 125.1, 117.0, 108.5, 108.2, 46.0, 39.3, 30.4, 28.6, 23.7, 23.1, 14.1, 10.6; MALDI-TOF MS *m*/*z*: calcd for $C_{66}H_{80}N_4O_4S_6$, 1185.8; found, 1185.8.

2.2.3. Synthesis of Ph2(TDPP)$_2$

Ph2(TDPP)$_2$ was synthesized by the Suzuki coupling. The compounds 1 (200 mg, 0.33 mmol), 4 (67 mg, 0.17 mmol), and $Pd(PPh_3)_4$ (19 mg, 0.02 mmol) were dissolved in a mixture of aqueous K_2CO_3 solution (2 M, 3 mL) and toluene (10 mL). After the solution was purged with N_2 for 20 min, 3 drops of Aliguat 336 were added. The reaction mixture was stirred at 110 °C for 24 h and then cooled down to room temperature. The reaction mixture was poured into acidic methanol (200 mL methanol and 10 mL HCl) and stirred for 1 h to remove the metal catalyst. The crude product purified by column chromatography on silica gel (100% $CHCl_3$ as eluent). The product Ph2(TDPP)$_2$ was obtained as a reddish blue solid (120 mg, 60% yield). ^{1}H NMR (300 MHz, $CDCl_3$,δ): 8.98 (d, *J* = 4.1 Hz, 2H), 8.90 (d, *J* = 3.5 Hz, 2H), 7.78 (d, *J* = 8.4 Hz, 4H), 7.70 (d, *J* = 8.4 Hz, 4H), 7.62 (d, *J* = 5.0 Hz, 2H), 7.53 (d, *J* = 4.1 Hz, 2H), 7.28 (d, *J* = 4.3 Hz, 2H), 4.09–4.04 (m, 8H), 1.95–1.88 (m, 4H), 1.42–1.28 (m, 32H), 0.95–0.88 (m, 24H); ^{13}C NMR (500 MHz, $CDCl_3$,δ): 161.8, 149.1, 140.4, 140.2, 140.1, 136.9, 135.2, 132.6, 130.5, 129.9, 129.0, 128.44 127.6, 126.7, 124.7, 108.2, 46.0, 39.3, 39.1, 30.4, 30.3, 28.6, 28.4, 23.74 23.6, 23.1, 23.1, 14.1, 14.0, 10.6, 10.5; MALDI-TOF MS *m*/*z*: calcd for $C_{72}H_{86}N_4O_4S_4$, 1199.7; found, 1199.7.

2.2.4. Synthesis of NPT(TDPP)$_2$

The same procedure as for Ph2(TDPP)$_2$ was performed. When the compound 1 (200 mg, 0.33 mmol) was reacted with 5 (63 mg, 0.17 mmol) in the presence of $Pd(PPh_3)_4$ (19 mg, 0.02 mmol), the product NPT(TDPP)$_2$ was obtained as a deep blue solid (130 mg, 67% yield). ^{1}H NMR (300 MHz, $CDCl_3$,δ): 8.98 (d, *J* = 4.3 Hz, 2H), 8.91 (d, *J* = 3.8 Hz, 2H), 8.12 (s, 2H), 7.92 (d, *J* = 8.4 Hz, 2H), 7.82 (d, *J* = 8.7 Hz, 2H), 7.62 (d, *J* = 3.8 Hz, 4H), 7.27 (d, *J* = 9.3 Hz, 2H), 4.09–4.00 (m, 8H), 1.97–1.89 (m, 4H), 1.38–1.30 (m, 32H), 0.95–0.88 (m, 24H); ^{13}C NMR (500 MHz, $CDCl_3$,δ): 161.8, 149.3, 140.2, 136.8, 136.3, 133.4, 131.3, 130.5, 129.9, 129.3, 129.2, 128.5, 125.0, 124.7, 108.3, 108.2, 46.0, 39.33 39.1, 30.5, 30.3, 28.7, 28.4, 23.8, 23.6, 23.1, 23.1, 14.1, 14.0, 10.6, 10.5;

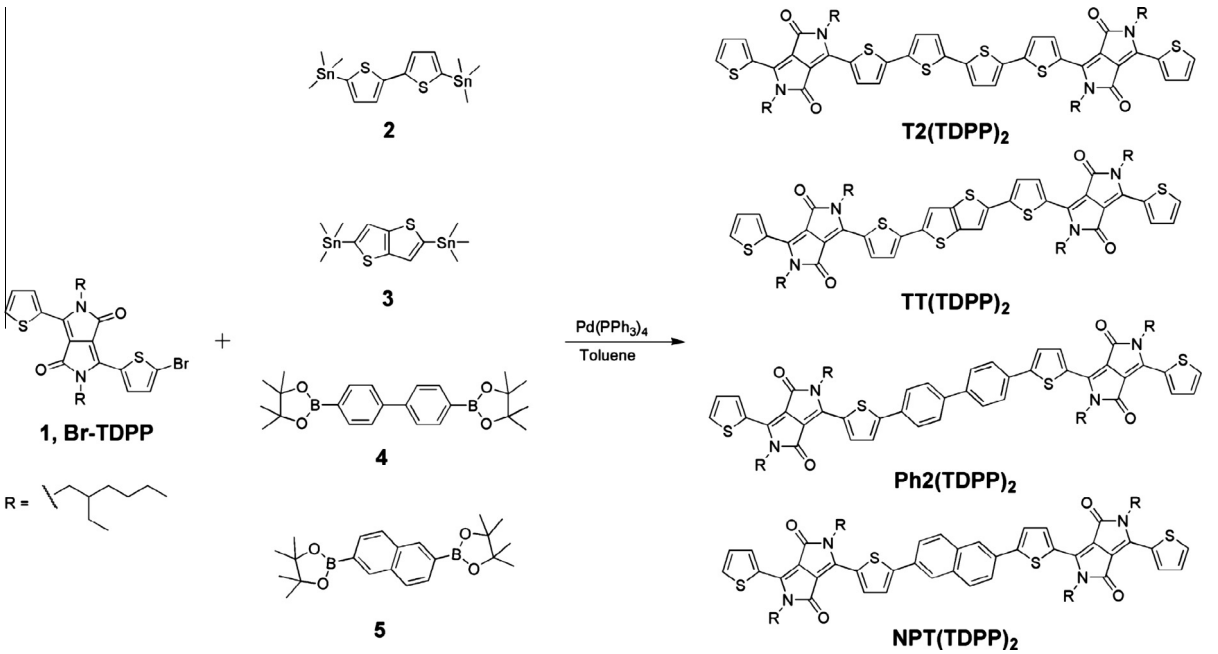

Scheme 1. Synthetic route of DPP-based small molecules.

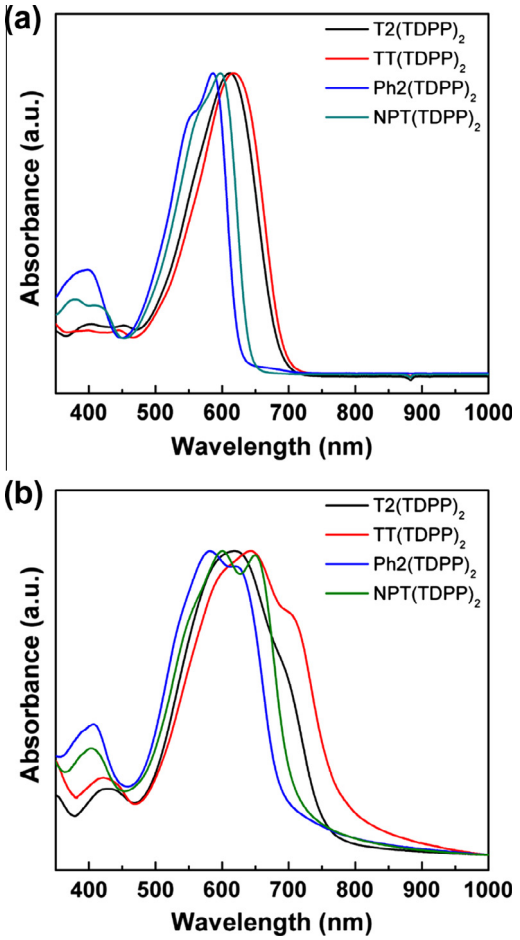

Fig. 2. UV–vis absorption spectra of SMs in (a) $CHCl_3$ solution and (b) in film state.

MALDI-TOF MS *m*/*z*: calcd for $C_{70}H_{84}N_4O_4S4$, 1173.7; found, 1173.3.

2.3. Characterization and measurement

The chemical structures of compounds were identified by ^1H NMR (Avance DPX-300) and ^{13}C NMR (Avance DPX-500). Molar masses of compounds were measured by matrix-assisted laser desorption/ionization time-of-flight (MALDI-TOF) mass spectrometer (Voyager-DE STR Biospectrometry Workstation, Applied Biosystem Inc.) with dithranol as a matrix. The optical absorption spectra were obtained by a UV–vis spectrophotometer (Lambda 25, Perkin Elmer). Cyclic voltammetry measurements were carried out using a potentiostat/galvanostat (VMP 3, Biologic) in an electrolyte solution of 0.1 M tetrabutylammonium hexafluorophosphate (Bu_4NPF_6) in dichloromethane. Platinum wires (Bioanalytical System Inc.) were used as both counter and working electrodes, and silver/silver ion (Ag in 0.1 M $AgNO_3$ solution, Bioanalytical System Inc.) was used as a reference electrode. The HOMO energy level of compound was calculated by using the equation: HOMO = $-[E_{ox}\ E_{1/2(ferrocene)} + 4.8]$ eV, where E_{ox} is the onset of oxidation potential of compound and $E_{1/2(ferrocene)}$ is the onset oxidation potential of ferrocene vs. Ag/Ag^+. The LUMO energy level was also calculated by using the equation: LUMO = $-[E_{red}\ E_{1/2(ferrocene)} + 4.8]$ eV, where E_{red} is the onset reduction potential of compound. X-ray diffractograms were obtained from an X-ray diffractometer (New D8 Advance, Bruker) using Cu Kα (λ = 1.54 Å) radiation. The morphology of active layer films was observed by TEM (JEM-1010, JEOL) with an accelerating voltage of 80 kV.

Table 1
Optical and electrochemical properties of SMs.

SMs	UV–vis absorption		E_g^{opt} (eV)[a]	HOMO (eV)	LUMO (eV)	E_g^{el} (eV)[b]
	λ_{max} ($CHCl_3$) (nm)	λ_{max} (film) (nm)				
$T2(TDPP)_2$	612	620, 686	1.65	−5.14	−3.55	1.5 9
$TT(TDPP)_2$	618	643, 702	1.60	−5.11	−3.56	1.5 4
$Ph2(TDPP)_2$	586	583, 620	1.80	−5.21	−3.57	1.6 4
$NPT(TDPP)_2$	597	600, 650	1.75	−5.18	−3.58	1.6

[a] Determined from the onset of UV–vis absorption spectra.
[b] Determined from cyclic voltammetry.

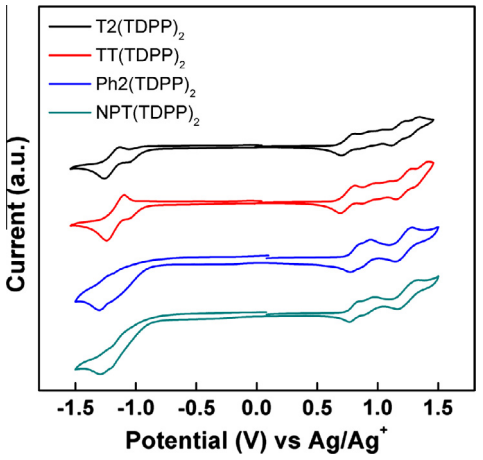

Fig. 3. Cyclic voltammograms of SMs.

2.4. Fabrication and characterization of photovoltaic cells

The organic solar cells were fabricated with the standard device configuration of glass/ITO/PEDOT:PSS/SM:$PC_{71}BM$/Ca/Al. Prior to device fabrication, the ITO-coated glass was cleaned with acetone and then isopropyl alcohol for 20 min. After complete drying at 120 °C for 30 min, the ITO-coated glass was treated with UV-ozone for 5 min. PEDOT:PSS was spin-coated on the ITO glass at 4000 rpm for 40 s and annealed at 120 °C for 30 min to yield a 40 nm thick film. The devices were transferred into a glove-box filled with N_2. A 1.5 wt% blend solution of SM:$PC_{71}BM$ was dissolved in $CHCl_3$ only or $CHCl_3$ with 0.5 vol% 1,8-diiodooctane (DIO) as a solvent additive. The

Table 2
Photovoltaic properties of BHJ solar cells under AM 1.5G illumination and charge carrier mobility under dark condition.

SMs	SM:$PC_{71}BM$ (w/w)[a]	μ_h ($cm^2\ V^{-1}\ s^{-1}$)[b]	J_{SC} ($mA\ cm^2$)	V_{OC} (V)	FF	PCE (%)
$T2(TDPP)_2$	1:1	5.1×10^{-4}	6.8	0.78	0.57	3.0
$TT(TDPP)_2$	1:1	7.7×10^{-4}	9.3	0.81	0.53	4.0
$Ph2(TDPP)_2$	1.5:1	6.1×10^{-4}	8.3	0.86	0.53	3.8
$NPT(TDPP)_2$	1:1	1.1×10^{-3}	9.5	0.87	0.53	4.4

[a] 0.5 vol% DIO added to the solution.
[b] Measured by SCLC method.

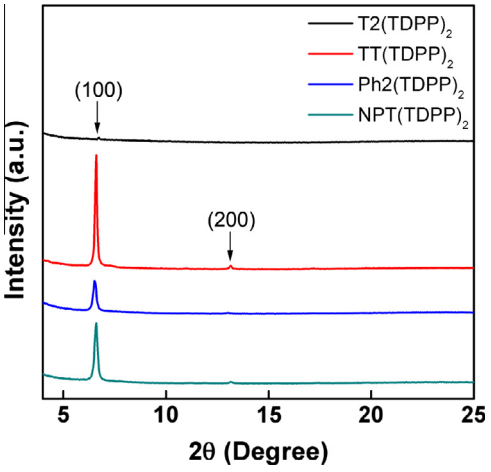

Fig. 4. X-ray diffractograms of SMs in thin film.

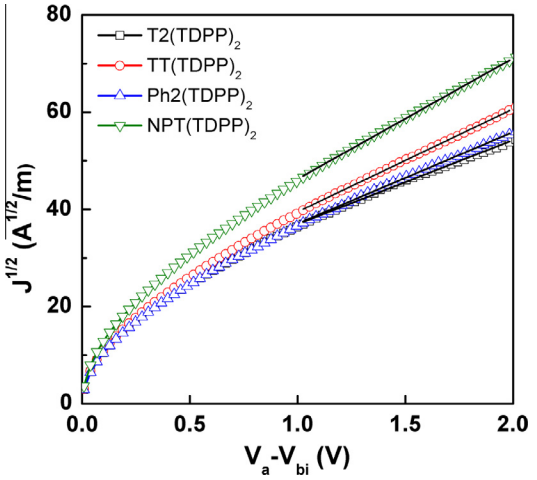

Fig. 5. Dark *J–V* characteristics of $T2(TDPP)_2$:$PC_{71}BM$ (1:1 w/w), $TT(TDPP)_2$:$PC_{71}BM$ (1:1 w/w), $Ph2(TDPP)_2$:$PC_{71}BM$ (1.5:1 w/w), and $NPT(TDPP)_2$:$PC_{71}BM$ (1:1 w/w) blends with hole-only device. The solid lines represent the best linear fit of the data points.

solution was stirred at 35 °C for 6 h and then passed through a 0.2 μm PTFE syringe filter before spin-coating. The solution was spin-coated on the top of PEDOT:PSS at 4000 rpm for 40 s. Finally calcium (20 nm) and then aluminium (100 nm) was thermally evaporated on the top of the active layer under vacuum (<10^{-6} Torr). The current

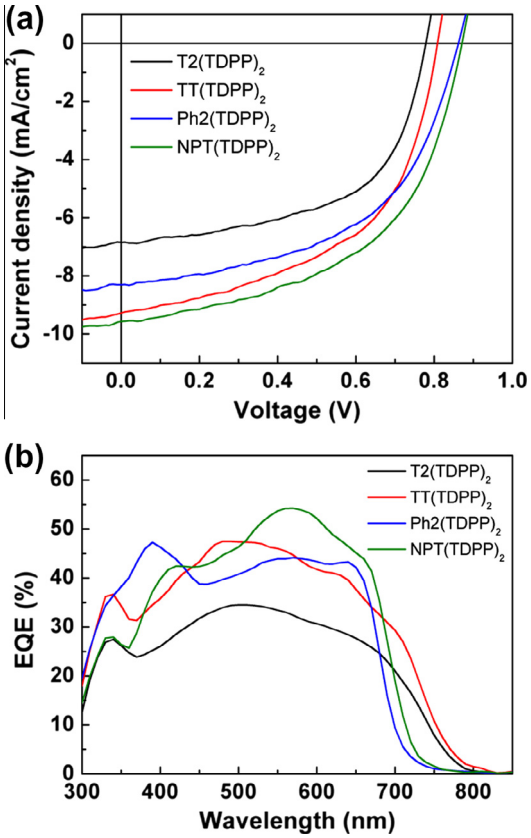

Fig. 6. (a) *J–V* curves of SMs/$PC_{71}BM$ BHJ solar cells under AM 1.5G, 100 mW cm^{-2} and (b) EQE spectra of the solar cells; $PC_{71}BM$ was used as an acceptor material.

density voltage (*J–V*) characteristics were measured with a Keithley 4200 source-meter under AM 1.5 G (100 mW cm^{-2}) simulated by a Newport–Oriel solar simulator. The light intensity was calibrated using a NREL certified photodiode and a light source meter prior to each measurement. The active area was 4 mm^2. The EQE was measured using a lock-in amplifier with a current preamplifier (K3100, McScience Co.) under short circuit current state with illumination of monochromatic light. The hole-only devices were fabricated with a device configuration of glass/ITO/PEDOT:PSS/SM:$PC_{71}BM$/Au. The hole mobilities of blend films were measured with the devices prepared from the identical condition with optimized photovoltaic cells and calculated from the space-charge limited *J–V* curve using the Mott–Gurney law.

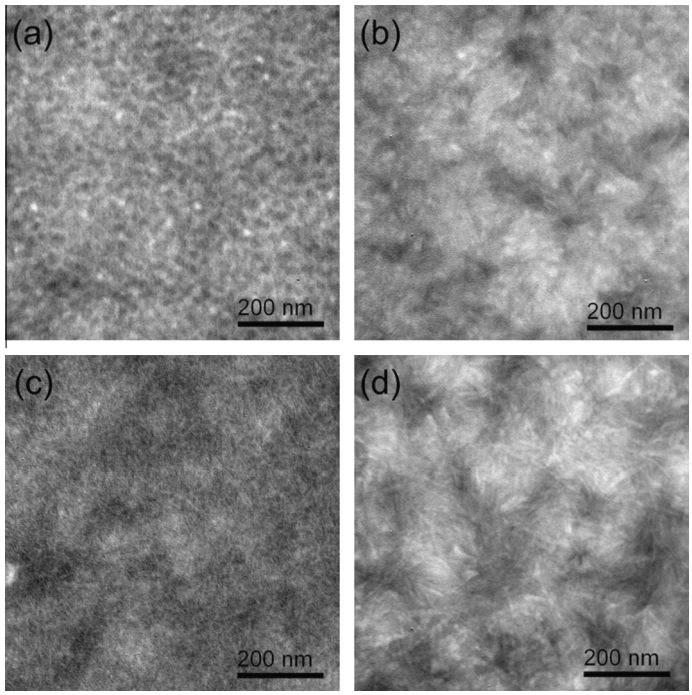

Fig. 7. TEM images of (a) T2(TDPP)$_2$:PC$_{71}$BM (1:1 w/w), (b) TT(TDPP)$_2$:PC$_{71}$BM (1:1 w/w), (c) Ph2(TDPP)$_2$:PC$_{71}$BM (1.5:1 w/w), and (d) NPT(TDPP)$_2$:PC$_{71}$BM (1:1 w/w) blends.

3. Results and discussion

The synthetic routes for four SMs with A–D–A structure, T2(TDPP)$_2$, TT(TDPP)$_2$, Ph2(TDPP)$_2$, and NPT(TDPP)$_2$, are outlined in Scheme 1. T2(TDPP)$_2$ and TT(TDPP)$_2$ were synthesized by the Stille cross-coupling reaction, whereas Ph2(TDPP)$_2$ and NPT(TDPP)$_2$ were synthesized by the Suzuki cross-coupling. The introduction of the branched 2-ethylhexyl group in SMs ensures the solubility in common solvents such as toluene, chloroform ($CHCl_3$), and dichloromethane.

The UV–vis absorption spectra of four SMs in $CHCl_3$ solution and thin film state are shown in Fig. 2, and the spectroscopic data are summarized in Table 1. All of SMs show a strong and broad absorption peak at longer wavelength originated from the intramolecular charge transfer between D and A units in SMs and a weak absorption peak at shorter wavelength attributed to $\pi-\pi$ transition. Such absorption spectra are the typical feature of donor-acceptor type conjugated molecules [40]. The onset of absorption (λ_{onset}) of T2(TDPP)$_2$ and TT(TDPP)$_2$ in solution is red-shifted by ~50 nm as compared to Ph2(TDPP)$_2$ and NPT(TDPP)$_2$ due to longer effective conjugation length afforded by thiophene derivatives in SMs as compared to phenylene derivatives. The absorption spectra in solid state exhibit the red-shift of the maximum absorption (λ_{max}) and the λ_{onset} relative to the solution state. Particularly, TT(TDPP)$_2$ and NPT(TDPP)$_2$ exhibit a discernible vibronic shoulder peak, indicating that TT(TDPP)$_2$ and NPT(TDPP)$_2$ are more effectively packed in solid state due to more planar structure of fused aromatic ring. When the optical bandgap (E_g^{opt}) is estimated from λ_{onset}, the E_g^{opt} of the T2(TDPP)$_2$ (1.65 eV) is lower than that of Ph2(TDPP)$_2$ (1.80 eV), as listed in Table 1. This is because the torsional angle between the two thiophene units in T2(TDPP)$_2$ is smaller than that between the two phenylene units in Ph2(TDPP)$_2$ and thereby T2(TDPP)$_2$ has more extended delocalization of electrons [41].

The HOMO and LUMO energy levels are also measured by cyclic voltammetry (CV), as shown in Fig. 3, and the results are summarized in Table 1. It has generally been accepted that the HOMO and the LUMO energy levels of D–A type conjugated molecules are mainly governed by those of D and A units, respectively. In other words, the weak donating unit in D–A molecule lowers the HOMO energy level while the weak accepting unit raises the LUMO energy level, and vice versa. Since the electron-donating power of phenylene is weaker than that of thiophene, the HOMO energy levels of Ph2(TDPP)$_2$ (−5.21 eV) and NPT(TDPP)$_2$ (−5.18 eV) are lower than those of T2(TDPP)$_2$ (−5.14 eV) and TT(TDPP)$_2$ (−5.11 eV), respectively. As a result, the V_{OC}s of Ph2(TDPP)$_2$ and NPT(TDPP)$_2$ are higher than those of T2(TDPP)$_2$ and TT(TDPP)$_2$, as listed in Table 2, because the V_{OC} is proportional to the energy difference between the HOMO of electron donor and the LUMO of electron acceptor in active layer of BHJ solar cells. It is noted that the LUMO energy levels of four SMs are nearly the same (−3.55 to −3.57 eV), because all SMs have the identical electron-accepting unit (DPP).

When the crystallinity of SMs was examined by X-ray diffraction (XRD), as shown Fig. 4, all SMs except for T2(TDPP)$_2$ showed a sharp diffraction peak at $2\theta = 6.6°$ corresponding to the interlayer *d*-spacing. Furthermore, TT(TDPP)$_2$ and NPT(TDPP)$_2$ with fused aromatic ring showed discernibly the second XRD peak at $2\theta = 13.2°$, indicating that these two SMs have higher crystallinity, which is primarily due to planarity of fused aromatic ring.

The space-charge limited current (SCLC) *J–V* curves were obtained in the dark condition using hole-only device fabricated under the identical condition with optimized photovoltaic cells (Fig. 5). When the hole mobility was estimated from the SCLC *J–V* curve using the Mott–Gurney law, the hole mobilities of TT(TDPP)$_2$ and NPT(TDPP)$_2$ are higher than those of T2(TDPP)$_2$ and Ph2(TDPP)$_2$, as listed in Table 2. These higher hole mobilities of TT(TDPP)$_2$ and NPT(TDPP)$_2$ may arise mainly from higher crystallinity due to more planar structure of fused aromatic units in the SMs.

The *J–V* curves of photovoltaic devices fabricated from the blends of SMs and $PC_{71}BM$ are shown in Fig. 6a and their photovoltaic properties are summarized in Table 2. The J_{SC}s of TT(TDPP)$_2$ and NPT(TDPP)$_2$ are higher than those of T2(TDPP)$_2$ and Ph2(TDPP)$_2$ primarily due to their higher hole mobility, while the V_{OC}s of Ph2(TDPP)$_2$ and NPT(TDPP)$_2$ are higher than those of T2(TDPP)$_2$ and TT(TDPP)$_2$ owing to weaker electron-donating power of phenylenes. As a result, NPT(TDPP)$_2$ exhibits the highest PCE of 4.4% with a J_{SC} of 9.5 mA cm^{-2}, a V_{OC} of 0.87 V, and a fill factor (FF) of 0.53. The external quantum efficiency (EQE) spectra (Fig. 6b) of optimized devices are nearly consistent with the absorption spectra (Fig. 2a). When the J_{SC} of NPT(TDPP)$_2$ was calculated from integration of EQE spectrum, the value of J_{SC} was 9.3 mA cm^{-2}, which is well consistent with J_{SC} measured from *J–V* curve.

When the morphologies of SM/$PC_{71}BM$ blend films prepared from $CHCl_3$/DIO solution are examined by TEM, as shown in Fig. 7, the blend films of TT(TDPP)$_2$ and NPT(TDPP)$_2$ with fused aromatic rings exhibit needle-like nanoscale phase separation, which is beneficial for charge carrier transport, while the blends of T2(TDPP)$_2$ and Ph2(TDPP)$_2$ show sphere-like nanoscale domain. However, when the blend films prepared from $CHCl_3$ without addition of DIO, the morphologies of T2(TDPP)$_2$ and Ph2(TDPP)$_2$ blends show homogeneous morphology, while TT(TDPP)$_2$ and NPT(TDPP)$_2$ blends show largely aggregated domains, both of which do not form the pathway for charge carrier transport (Fig. S5). Hence, it is realized that the addition of solvent additive (DIO) largely affects the blend morphology.

4. Conclusions

For enhancement of both J_{SC} and V_{OC} of DPP-based SMs, a series of SMs with A–D–A type structure, where A is DPP and D is different electron-donating units, are synthesized and their photovoltaic properties are compared. Ph2(TDPP)$_2$ and NPT(TDPP)$_2$ with weak electron-donating unit show deeper HOMO levels than T2(TDPP)$_2$ and TT(TDPP)$_2$ with strong electron-donating unit. As a consequence, the photovoltaic cells based on Ph2(TDPP)$_2$ and NPT(TDPP)$_2$ exhibit higher V_{OC} than T2(TDPP)$_2$ and TT(TDPP)$_2$ cells. The introduction of fused aromatic ring (TT and NPT) in SMs lowers the bandgap and enhances hole mobility mainly due to high crystallinity derived from planar structure of fused aromatic ring. As a result, TT(TDPP)$_2$ and NPT(TDPP)$_2$ exhibit higher J_{SC}s than T2(TDPP)$_2$ and Ph2(TDPP)$_2$. As a consequence, the introduction of NPT, which lowers the HOMO energy level and enhances hole mobility, affords the highest PCE of 4.4% with a V_{OC} of 0.87 V, a J_{SC} of 9.5 mA cm^{-2}, and a FF of 0.53. This successful result provides a guideline for rational design of conjugated small molecules for enhancement of both V_{OC} and J_{SC}.

Acknowledgements

The authors thank the Ministry of Education, Science and Technology (MEST), Korea for financial support through the Global Research Laboratory (GRL) and the World Class University (WCU) programs.

Appendix A. Supplementary material

Supplementary data associated with this article can be found, in the online version, at http://dx.doi.org/10.1016/j.orgel.2013.03.031.

References

[1] C.J. Brabec, N.S. Sariciftci, J.C. Hummelen, Adv. Funct. Mater. 11 (2001) 15–26.
[2] H. Spanggaard, F.C. Krebs, Sol. Energy Mater. Sol. Cells 83 (2004) 125–146.
[3] S. Günes, H. Neugebauer, N.S. Sariciftci, Chem. Rev. 107 (2007) 1324–1338.
[4] B.C. Thompson, J.M.J. Fréchet, Angew. Chem. Int. Ed. 47 (2008) 58–77.
[5] F.C. Krebs, Sol. Energy Mater. Sol. Cells 93 (2009) 394–412.
[6] J.W. Jung, W.H. Jo, Adv. Funct. Mater. 20 (2010) 2355–2363.
[7] M. Helgesen, R. Søndergaard, F.C. Krebs, J. Mater. Chem. 20 (2010) 36–60.
[8] F.C. Krebs, J. Fyenbo, M. Jørgensen, J. Mater. Chem. 20 (2010) 8994–9001.
[9] J.W. Jung, F. Liu, T.P. Russell, W.H. Jo, Energy Environ. Sci. 5 (2012) 6857–6861.
[10] J.W. Jo, S.S. Kim, W.H. Jo, Org. Electron. 13 (2012) 1322–1328.
[11] T.S. Poll, J.A. Love, T.Q. Nguyen, G.C. Bazan, Adv. Mater. 24 (2012) 3646–3649.
[12] J. Zhou, X. Wan, Y. Liu, Y. Zuo, Z. Li, G. He, G. Long, W. Ni, C. Li, X. Su, Y. Chen, J. Am. Chem. Soc. 134 (2012) 16345–16351.
[13] Y. Sun, G.C. Welch, W.L. Leong, C.J. Takacs, G.C. Bazan, A.J. Heeger, Nat. Mater. 11 (2012) 44–48.
[14] Z. He, C. Zhong, X. Huang, W.Y. Wong, H. Wu, L. Chen, S. Su, Y. Cao, Adv. Mater. 23 (2011) 4636–4643.
[15] J. Huang, C. Zhan, X. Zhang, Y. Zhao, Z. Lu, H. Jia, B. Jiang, J. Ye, S. Zhang, A. Tang, Y. Liu, Q. Pei, J. Yao, ACS Appl. Mater. Int. (2011), http://dx.doi.org/10.1021/am302786u.
[16] C.E. Small, S. Chen, J. Subbiah, C.M. Amb, S.W. Tsang, T.H. Lai, J.R. Reynolds, F. So, Nat. Photonics 6 (2012) 115–120.
[17] X. Li, W.C.H. Choy, L. Huo, F. Xie, E.I. Sha, B. Ding, X. Guo, Y. Li, J. Hou, J. You, Y. Yang, Adv. Mater. 24 (2012) 3046–3052.
[18] Z. He, C. Zhong, S. Su, M. Xu, H. Wu, Y. Cao, Nat. Photonics 6 (2012) 591–595.
[19] Z.G. Zhang, J. Wang, J. Mater. Chem. 22 (2012) 4178–4187.
[20] M.C. Scharber, D. Mühlbacher, M. Koppe, P. Denk, C. Waldauf, A.J. Heeger, C.J. Brabec, Adv. Mater. 18 (2006) 789–794.
[21] O.P. Lee, A.T. Yiu, P.M. Beaujuge, C.H. Woo, T.W. Holcombe, J.E. Millstone, J.D. Douglas, M.S. Chen, J.M.J. Fréchet, Adv. Mater. 23 (2011) 5359–5363.
[22] J.H. Seo, Syn. Metals 162 (2012) 748–752.
[23] I. McCulloch, M. Heeney, C. Bailey, K. Genevicius, I. Macdonald, M. Shkunov, D. Sparrowe, S. Tierney, R. Wagner, W. Zhang, M.L. Chabinyc, R.J. Kline, M.D. McGehee, M.F. Toney, Nat. Mater. 5 (2006) 328–333.
[24] J.S. Wu, Y.J. Cheng, M. Dubosc, C.H. Hsieh, C.Y. Chang, C.S. Hsu, Chem. Commun. 46 (2010) 3259–3261.
[25] K. Takimiya, S. Shinamura, I. Osaka, E. Miyazaki, Adv. Mater. 23 (2011) 4347–4370.
[26] Y. Lee, Y.M. Nam, W.H. Jo, J. Mater. Chem. 21 (2011) 8583–8590.

[27] J.S. Lee, S.K. Son, S. Song, H. Kim, D.R. Lee, K. Kim, M.J. Ko, D.H. Choi, B. Kim, J.H. Cho, Chem. Mater. 24 (2012) 1316–1323.
[28] P. Sonar, S.P. Singh, Y. Li, Z.E. Ooi, T.J. Ha, I. Wong, M.S. Soh, A. Dodabalapur, Energy Environ. Sci. 4 (2011) 2288–2296.
[29] E. Zhou, S. Yamakawa, K. Tajima, C. Yang, K. Hashimoto, Chem. Mater. 21 (2009) 4055–4061.
[30] E. Zhou, Q. Wei, S. Yamakawa, Y. Zhang, K. Tajima, C. Yang, K. Hashimoto, Macromolecules 43 (2010) 821–826.
[31] E. Zhou, J. Cong, K. Hashimoto, K. Tajima, Energy Environ. Sci. 5 (2012) 9756–9759.
[32] B. Walker, A.B. Tamayo, X.D. Dang, P. Zalar, J.H. Seo, A. Garcia, M. Tantiwiwat, T.Q. Nquyen, Adv. Funct. Mater. 19 (2009) 3063–3069.
[33] S. Loser, C.J. Bruns, H. Miyauchi, R.P. Ortiz, A. Facchetti, S.I. Stupp, T.J. Marks, J. Am. Chem. Soc. 133 (2011) 8142–8145.
[34] L. Zhang, S. Zeng, L. Yin, C. Ji, K. Li, Y. Li, Y. Wang, New J. Chem. 37 (2013) 632–639.
[35] B. Walker, J. Liu, C. Kim, G.C. Welch, J.K. Park, J. Lin, P. Zalar, C.M. Proctor, J.H. Seo, G.C. Bazan, T.Q. Nguyen, Energy Environ. Sci. 6 (2013) 952–962.
[36] J.W. Lee, Y.S. Choi, W.H. Jo, Org. Electron. 13 (2012) 3060–3066.
[37] Y. Zhang, C. Kim, J. Lin, T.Q. Nguyen, Adv. Funct. Mater. 97 (2012) 97–105.
[38] X. Zhang, L.J. Richter, D.M. DeLongchamp, R.J. Kline, M.R. Hammond, I. McCulloch, M. Heeney, R.S. Ashraf, J.N. Smith, T.D. Anthopoulos, B. Schroeder, Y.H. Geerts, D.A. Fischer, M.F. Toney, J. Am. Chem. Soc. 133 (2011) 15073–15084.
[39] F. Mo, Y. Jiang, D. Qiu, Y. Zhang, J. Wang, Angew. Chem. Int. Ed. 49 (2010) 1846–1849.
[40] Z.B. Henson, G.C. Welch, T. Poll, G.C. Bazan, J. Am. Chem. Soc. 134 (2011) 3766–3779.
[41] H.J. Son, F. He, B. Carsten, L. Yu, J. Mater. Chem. 31 (2011) 18934–18945.